Morphology–Permeability Relationships in Biaxially Oriented Pet Films: A Relationship Between Oxygen Permeability and PROF

RAMESH M. GOHIL

Du Pont, Circleville Research Laboratory, Circleville, Ohio 43113

SYNOPSIS

The effect of uniaxial and biaxial film-processing parameters on the orientation of the phenyl ring in the crystalline and amorphous phases has been evaluated using a variety of techniques. It has been demonstrated that the total phenyl ring orientation factor (PROF) measured from refractive indices can reflect the nature of amorphous and crystalline phases as well as morphological changes taking place due to variation in processing conditions. The PROF parameter can, therefore, offer a useful relationship to predict oxygen permeability for biaxially oriented PET films prepared under a variety of processing conditions. The cause of nonlinearity of oxygen permeability with birefringence, percent crystallinity, and tan δ maximum peak temperature (MPT) is discussed in detail. © 1993 John Wiley & Sons, Inc.

INTRODUCTION

In the past, extensive studies have been carried out to understand the role of various parameters on the permeability of gases through polymeric films.[1-5] A major study focused on the glassy and rubbery state of polymers, for which the diffusion processes above and below the glass transition temperature are different. There is increasing interest to study biaxially oriented semicrystalline polymers like PET films, mainly due to technological demands.[2,6,7] However, the treatment of the problem in such a heterogeneous system is more complex and there presently is no simple model to describe gas permeation.[8] Recent reports by Ward et al.[8,9] summarize some important variables.

As the morphology of an oriented semicrystalline polymer is controlled by the stretching conditions and heat treatment, so will the gas permeability also change. It is therefore difficult to develop a unified theory to describe gas permeability, and it may be desirable to look for a structural parameter that correlates well with this phenomenon. The major intention of the present study was to search for a single universal parameter that could predict oxygen permeability through biaxially oriented PET film prepared under a variety of processing conditions.

Journal of Applied Polymer Science, Vol. 48, 1649–1664 (1993)
 CCC 0021-8995/93/091649-16

EXPERIMENTAL

Film-stretching Process

The uniaxial (UNI), biaxial sequential (SEQ), and simultaneous (SIM) stretching processes are schematically shown in Figure 1.

The stretching operations were conducted at 95°C on a T.M. Long stretcher having a 4 × 4 inch pantograph capable of stretching up to 4.0× in both directions. In the sequential stretching process, an amorphous cast film was first stretched along a direction usually defined as the machine direction (MD) with a transverse direction (TD) restraint up to a draw ratio of 3.5×. Uniaxial stretching was carried out using amorphous cast films with constant width to a desired draw ratio at 95°C with a stretching rate of 9000%/min. After completion of uniaxial stretching, in the second step, the film was stretched in the TD to a desired draw ratio (Fig. 1). The TD draw is nothing more than the stretching of a crystalline film in the direction of minimum molecular

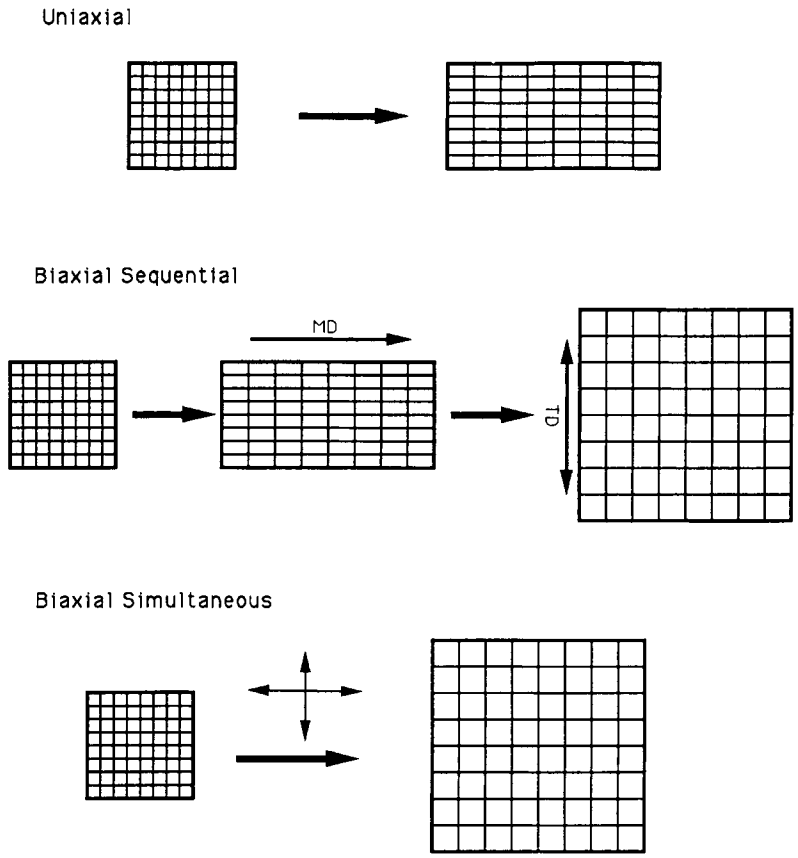

Figure 1 Schematic representation of various stretching processes: (a) uniaxial; (b) biaxial stretching; (c) simultaneous biaxial stretching.

orientation. Thus, the purpose of TD stretching of a uniaxially stretched film is to minimize the film anisotropy, whereas a second deformation along the direction of maximum molecular orientation (two-stage uniaxial deformation) at an appropriate temperature could be used to achieve ultrahigh modulus.[10] In the simultaneous stretching process, MD× and TD× are varied at the same time to the desired level. Once the simultaneous process is started, deformation continues without interruption at a selected temperature. Subsequently, films were heat-set at 200°C for 5 min with fixed dimensions. Additive-free PET having a molecular weight ($\overline{M}_n$) of 20,000 was utilized for the study, and the diethylene glycol content (DEG) was 1.5 mol %.

Permeability Measurements

The apparatus used in the present work was a Mocon Ox-Tran Twin DL 200 oxygen permeability tester. Measurements were carried out at 25°C. A 4 × 4 in. film is placed between the two halves of the chamber, and the chamber and film sample are flushed with a carrier gas (nitrogen with a trace of hydrogen) to remove completely all traces of oxygen. In the cell, oxygen is introduced to one surface at a pressure of 1 atm and the oxygen emerging from the opposite surface is carried away by the carrier gas to a sensor, which gives a measurement of oxygen content. For other details, refer to Refs. 8, 11, and 12. All the reported permeabilities were normalized for the thickness of the individual films and expressed as cubic centimeters of gas transmitted through 100 sq in. of barrier per day at a pressure differential of 1 atmosphere and a thickness of 1 mil. It is denoted as cc-mil/100 sq in. 24 h-atm.

X-ray Pole Figures

A specimen for pole-figure determination is a square prism (right square cylinder) about 1 by 1 by 5 mm. It is prepared by stacking enough layers of film to

attain the 1 mm thickness and then trimming to 1 mm width. The sample integrity is maintained by coating the exposed edges with collodion.

The pole figures were obtained with a Picker "single-crystal" goniometer with Eulerian geometry and three axes (phi, chi, and two-theta) automated. Ni-filtered copper radiation was used as the X-ray source. Data obtained were processed by a Hewlett-Packard computer. A specimen is mounted in the instrument and aligned so that the MD is coincident with the direction $\chi = 90$ (the north pole–south pole axis) and the surface normal (SN) or "thickness direction" (ThD) is directed along $\phi = 0$, $\chi = 0$; the TD is then along $\phi = 90$, $\chi = 0$. The value for the pole figure for any phi–chi pair is determined by measuring the intensity at the two-theta value corresponding to the desired *hkl* reflection. For our procedure, this intensity is an approximation to the "integrated intensity" obtained by measuring the peak intensity via interpolation between low-angle and high-angle background intensities. The entire procedure is automated and phi–chi pairs are sampled in 10° increments in both ϕ and χ.

A detailed explanation of pole figures has been published previously.[13,14] As some of the notations we followed are different, it may be useful to summarize them in brief.

A pole figure is a representation of the angular distribution of "pole" or plane normals to a particular crystallographic plane, identified by its Miller indices, *hkl*. The coordinate system is equivalent to that of the earth with the angle ϕ corresponding to longitude (east–west) and the angle χ corresponding to latitude (north–south). A pole figure is shown as a stereographic projection, with the center corresponding to the north pole ($\chi = 90°$) and the outer circle corresponding to the equator ($\chi = 0°$; ϕ any value between 0 and 360°). The projected coordinate system shows increments of 30° in both ϕ (0, 30, 60 · · · 300, 330) and χ (0, 30, and 60). Any pole figure is shown as a contour plot superimposed on the coordinate grid.

To understand the details of the pole figures, it may be useful to define the MD, TD, and *c*-axis directions in the PET films with respect to the north–south pole. The film is schematically represented in Figure 2, in which the MD and TD directions are shown with the arrows. Plotted in a pole figure are the spherical projections of the plane normals drawn outward from the middle of the sphere; the arrows indicate north and south directions. The angles χ and ϕ define positions of (*hkl*) poles. Two different crystal orientations are also shown in Figure 2 where double arrows show molecular directions in the crystals. The circle represents the pole figure with the outer circle corresponding to the equator.

The best information regarding crystalline orientation can be obtained from pole figure analysis of the (100) and ($\bar{1}$05) planes (ca. 80° apart). The ($\bar{1}$05) reflection is the most suitable for monitoring this *c*-axis orientation. It is about 10° away from the *c*-axis direction, but essentially in the plane of the film, and can be used to determine the major *c*-axis direction, whether or not there is a secondary *c*-axis population, and how much of a spread there is in the *c*-axis orientation. In uniaxially oriented films, the *c*-axis (molecular direction) is mainly along the MD direction (along the north–south direction). In such a case, one observes intensity from ($\bar{1}$05) planes at the center of the pole figure (see the top part of Fig. 2). The spread in the intensity indicates deviation of the *c*-axis from the plane of the film. If the crystals are oriented along both directions, MD and TD, then additional intensity in the pole figure arises at both ends marked with "A" along the TD (Fig. 2). A film having an in-plane isotropic crystal orientation will show a continuous band of uniform intensity at the center of the pole figure (see heavy dotted lines).

In the triclinic unit cell of PET crystals, the phenyl ring (benzene ring) lies in the (100) plane. Therefore, the orientation of a phenyl ring with respect to the film plane can be determined from the orientation of the (100) plane. In the case of uniplanar film containing all the phenyl rings in the film plane, the (100) plane will lie in the film plane. Therefore, the intensity arising from the (100) planes will be in the direction perpendicular to the film plane. Thus, the intensity is expected to occur at the location marked with "B" in Figure 2. The spread in the intensity (angle ϕ) will ultimately determine the deviation from the film planarity.

The measurement of the (100) orientation factor (OF) was performed by measuring the half-width value ϕ from the diffraction intensity curve of the (100) diffraction and computing in the formula

$$\mathrm{OF}_{(100)} = \frac{180 - \phi}{\phi} \times 100 \qquad (1)$$

Phenyl Ring Orientation from Refractive Index

Information regarding the overall phenyl ring orientation in film can also be deduced from the values of refractive indices measured along different directions. Phenyl ring orientation, which, in fact, determines the film planarity, was defined[15] as

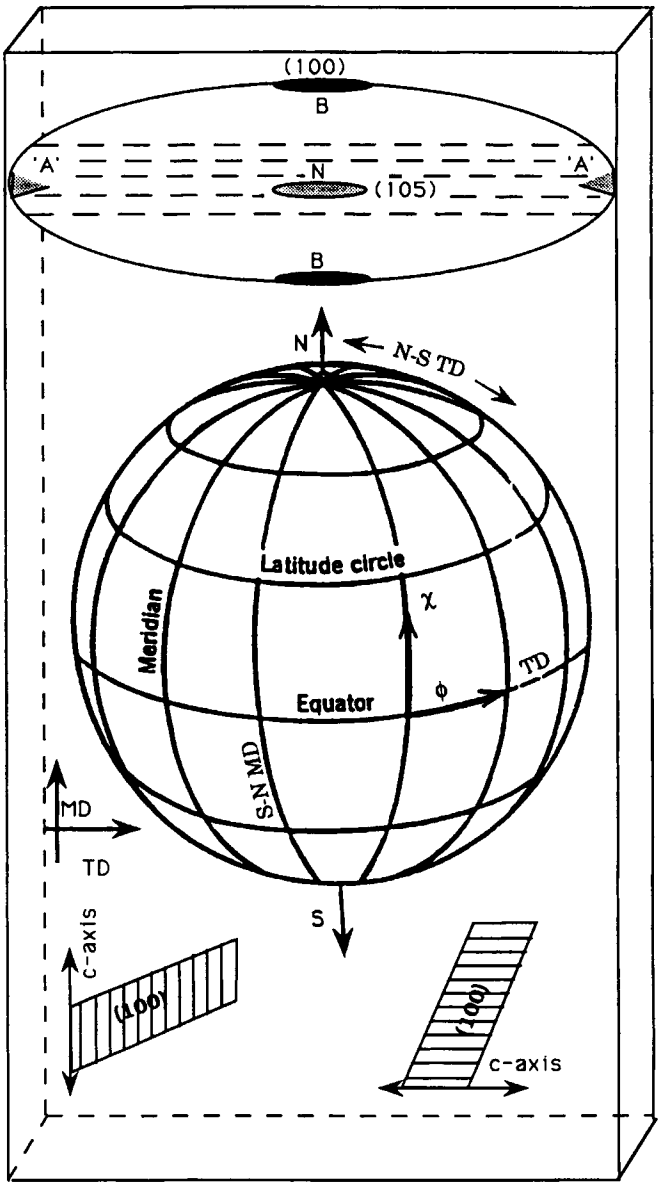

Figure 2 Schematic representation of pole figure with respect to the orientation of PET film. Note the relation between the occurrence of intensity in pole figures with the different stretching directions of the films.

$$\left[\frac{\eta_x + \eta_y}{2}\right] - \eta_z \qquad (2)$$

where η_x, η_y, and η_z are the refractive indices along the maximum, minimum, and thickness directions, and could also be measured along the MD, TD, and thickness directions (ThD). The values of this total phenyl ring orientation can be converted into a percentage using values of intrinsic refractive indices (η_x = 1.8034, η_y = 1.7728, η_z = 1.3688) reported previously.[16] The equation for the phenyl ring orientation factor (PROF) can be written as

$$\left[\left(\frac{\eta_x + \eta_y}{2} - \eta_z\right) \Big/ 0.42\right] \times 100 \qquad (3)$$

Changes in PROF reflect the relative orientation of the phenyl ring in crystalline and amorphous phases with respect to the film plane. In the past, several other procedures for measuring film planarity have

been published using refractive indices and infrared measurements.[9,17,18]

Intrinsic Fluorescence

Details regarding the experimental setup to measure intrinsic fluorescence were summarized in previous publications.[19–21] In the experiment, PET dimers are excited at a wavelength, λ = 340 nm, and with the polarizer and analyzer parallel, the specimen rotated. The intensity of fluorescence emission (at λ = 390 nm) exclusively occurring from the amorphous phase was measured every 10° of rotation, and polar plots of the in-plane angular distribution of polarized fluorescence intensity were thus obtained. The polar plots reveal the distribution of amorphous orientation in the plane of the film.

To quantify the proportion of crystalline chains oriented along the MD and TD, an "amorphous orientation ratio," AOR, was calculated as follows:

$$\mathrm{AOR_{MD}} = \frac{I_{\mathrm{MD}}}{I_{\mathrm{MD}} + I_{\mathrm{TD}}} \tag{4}$$

and

$$\mathrm{AOR_{TD}} = \frac{I_{\mathrm{TD}}}{I_{\mathrm{MD}} + I_{\mathrm{TD}}} \tag{5}$$

where I_{MD} and I_{TD} are the emission intensities obtained with, respectively, the machine and transverse draw directions of the film parallel to the polarization direction.

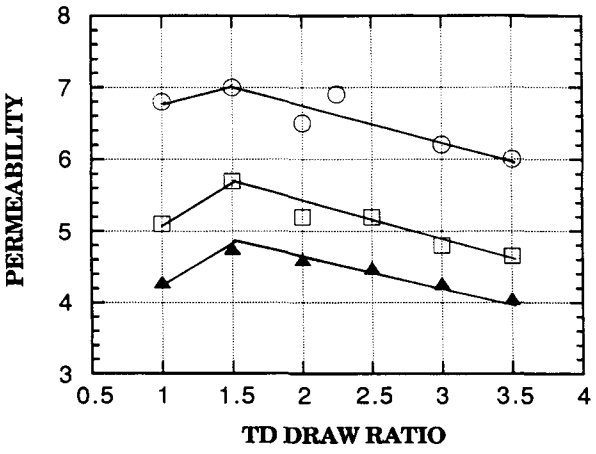

Figure 3 Oxygen permeability vs. TD draw ratio for sequentially stretched film heat-set at different conditions: (○) nonannealed and annealed at (□) 200°C and (▲) 170°C.

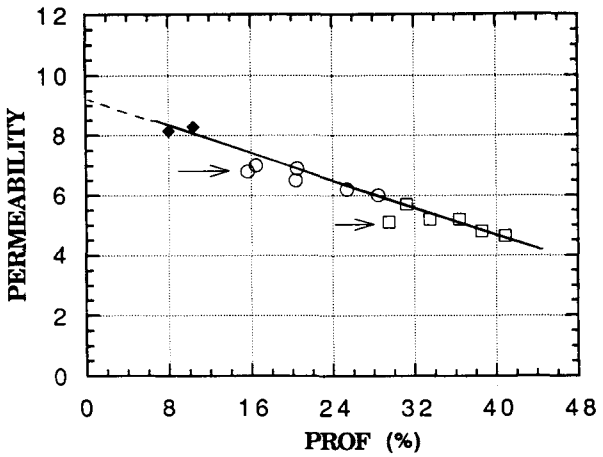

Figure 4 Oxygen permeability vs. phenyl ring orientation factor for sequentially stretched annealed and nonannealed films: (○) nonannealed, (□) 200°C; (♦) cast crystalline films. Values marked with arrows are from uniaxially stretched films.

Dynamic Mechanical Analysis

Dynamic mechanical analysis (DMA) was carried out on the instrument prepared by Polymer Lab DMTA in the temperature range of 0–250°C using a frequency of 1 Hz, a heating rate of 5°C/min, and sample dimensions of 5.67 × 2 mm.

Density Measurements

Densities of the PET films were obtained using a density gradient column made from toluene and carbon tetrachloride. The percentage crystallinities of the films were computed from

$$X_c = \frac{\rho_c(\rho - \rho_a)}{\rho(\rho_c - \rho_a)} \times 100 \tag{6}$$

where ρ is the sample density. The subscripts "c" and "a" denote the crystalline and amorphous phases. The density of the crystalline phase was taken as 1.445 g/cc, and the amorphous phase, as 1.335.[16]

RESULTS

Figure 3 shows the effect of the TD draw ratio on the permeability of oxygen on the PET films annealed at different temperatures. Note that annealing of stretched film at 170°C produces lower permeability than does annealing at 200°C. These re-

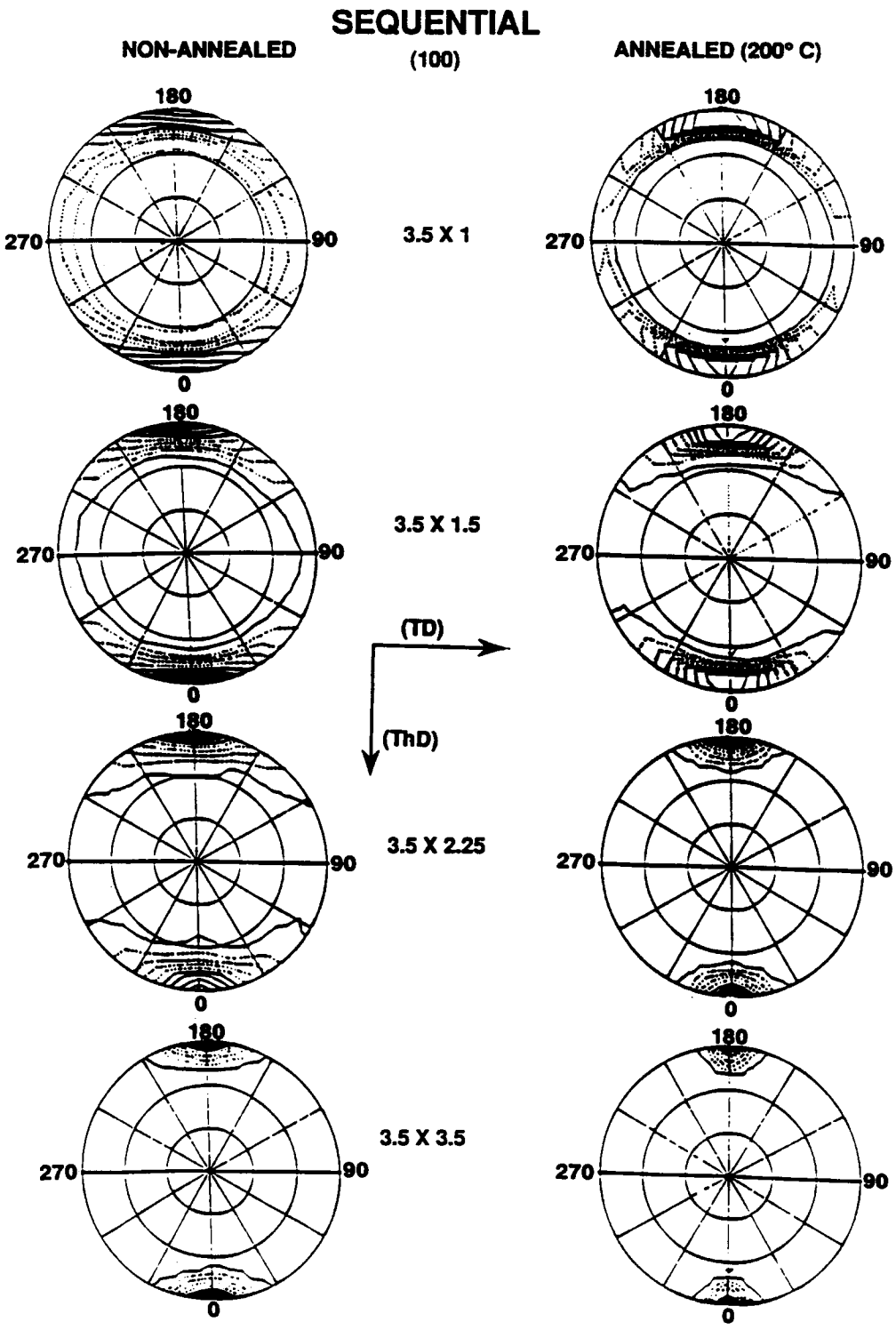

Figure 5(a) (100) pole figures obtained from the nonannealed and annealed (200°C) sequentially stretched films. TD stretch ratio for each film is indicated, while the MD stretch ratio is 3.5× for all the films. TD and ThD, respectively, represent the transverse and thickness directions of the films. (b) ($\bar{1}05$) pole figures obtained from the non-heat-set and heat-set (200°C) sequentially stretched films. TD stretch ratio for each film is indicated, while the MD stretch ratio is 3.5×.

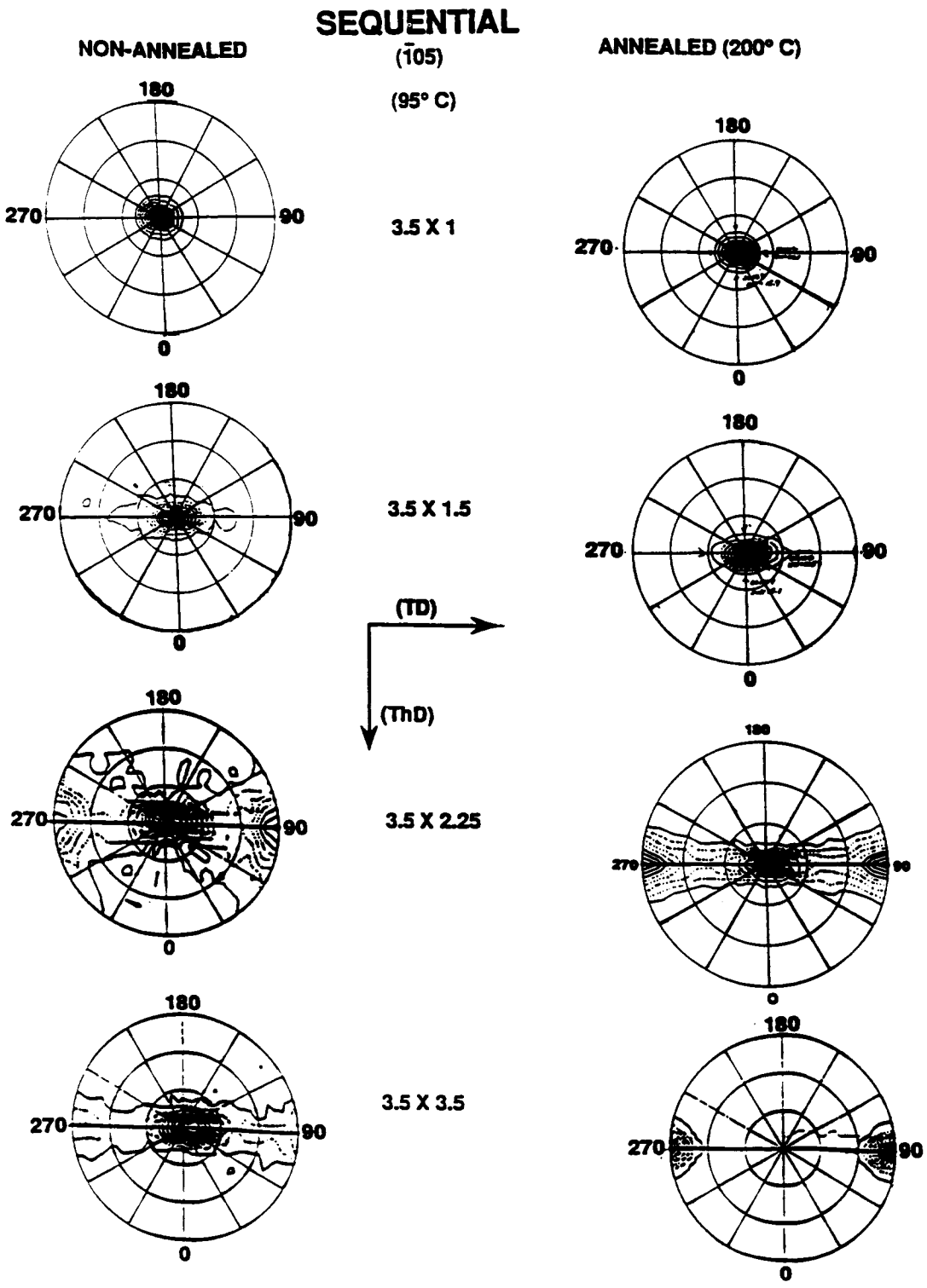

Figure 5(b) *(Continued from the previous page)*

sults are plotted against PROF (Fig. 4) and show a linear relationship. Our intention here is to understand the linearity of this relationship and also to find out whether such a relationship can be generalized for films prepared under a variety of processing conditions.

Gas permeability is the product of a solubility coefficient (S) and a coefficient of diffusion (D) (a

kinetic factor). For semicrystalline polymers, it is necessary to account for the impermeable crystalline phase (X_c).

$$P_{O_2} = S \cdot D \cdot (1 - X_c) \quad (7)$$

Equation (7) reflects the dependency on percent crystallinity and factors governing the state of the amorphous phase. Normally, the gas permeability and water vapor is correlated with percent crystallinity, and factors affecting diffusion of gases, from the amorphous phase. Such factors include amorphous birefringence, glass transition temperature, amorphous orientation function, etc.

First we will examine the variation in orientation of the (100) plane of PET crystals containing the phenyl ring with the processing parameters. Previously, this was defined as planarity.[22] Here we would like to limit the term "film planarity" to the orientation of the (100) crystal plane in PET crystallites. The variation of planarity will be then compared with the overall phenyl ring orientation in the amorphous and crystalline phases. This will allow us to extract some information about the changes taking place in the phenyl ring orientation in the amorphous phase.

Crystalline Phase Changes

In this study, changes in crystalline orientation were followed with wide-angle X-ray pole figures. The change in phenyl ring orientation with the TD draw can be deduced from the orientation of (100) planes of the PET crystals with respect to the film plane. Figure 5(a) shows pole figures for the (100) planes that indicate the phenyl ring orientation within the crystals. Each film was MD stretched to 3.5×, then TD stretched to the draw ratios shown in the figure, i.e., 1.0, 1.5, 2.25, and 3.5×. The pole figures on the left and right show the (100) plane orientation, respectively, before and after annealing (heat setting at 200°C). The spread in intensity arising from (100) planes along the TD is broad and decreases with the TD draw ratio. This suggests that with increasing TD draw the (100) planes lie in the film planes. Thus, the planarity of the film, defined earlier[22] in terms of crystalline orientation, increases with the TD draw ratio or planar draw ratio.

The (100) pole figures of annealed samples show a decrease in intensity spread at angle ϕ, indicating that planarity further increases with heat treatment. Thus, the (100) plane orientation (planarity) is also dependent on the time and temperature of heat treatment. In other words, perfection in crystal orientation with respect to the film plane improves with heat treatment.

The spread in the intensity arising from the (100) normals in the pole figures along the TD and MD is correlated with the TD draw ratio [Fig. 6(a)]. The spread of the (100) normal is greater toward the TD than toward the MD. The orientation of the (100) plane to the film plane improves with increasing TD draw. The realignment along the SN–TD azimuth is much more rapid than that along the SN–MD azimuth. Variation in the (100) plane orientation factor with TD draw ratio for annealed and nonannealed films is shown in Figure 6(b). Above a TD draw ratio of 1.5×, heat treatment at 200°C increases the (100) plane orientation of PET crystals over that of unannealed samples.

Figure 5(b) shows pole figures for the ($\bar{1}05$) planes that show the molecular chain axis orientation within the crystals. Again, each film was MD stretched by 3.5×, then TD stretched to the draw ratios shown in the figure, i.e., 1.0, 1.5, 2.25, and 3.5×. The pole figures on the left and right, respectively, show the ($\bar{1}05$) plane orientation before and after annealing (heat setting at 200°C).

The first film in this series is uniaxially stretched, i.e., 3.5 × 1.0×. The chain axes within the crystallites are aligned along the MD before and after annealing. The second film shows a similar orientation before and after annealing. At the TD draw ratio of 2.25×, one begins to see the bimodial crystalline orientation character; however, on heat-setting, this bimodal crystalline orientation becomes almost isotropic in the film plane. The pole figure of 3.5 × 3.5 drawn film shows bimodal character, but on heat treatment, MD oriented crystals start disappearing and a TD oriented texture develops, with the crystal c-axes oriented toward the TD. These results are in line with those of a previous wide angle X-ray study[23] and suggest that the population of crystallites with their c-axis along the MD and TD is influenced by the time and temperature of heat treatment.

The effect of heat treatment on percent crystallinity for samples stretched at various draw ratios is shown in Figure 7. The crystallinity of the nonannealed samples initially increases with the TD draw ratio up to 2.3×, then it decreases slightly. Matsumoto et al.[24] similarly noted this behavior. Annealing the films increases the crystallinity to ultimate values that show a slight decreasing trend with TD draw ratio. As seen from Figures 4 and 7, increasing crystallinity during heat treatment simultaneously leads to an increase in the values of PROF.

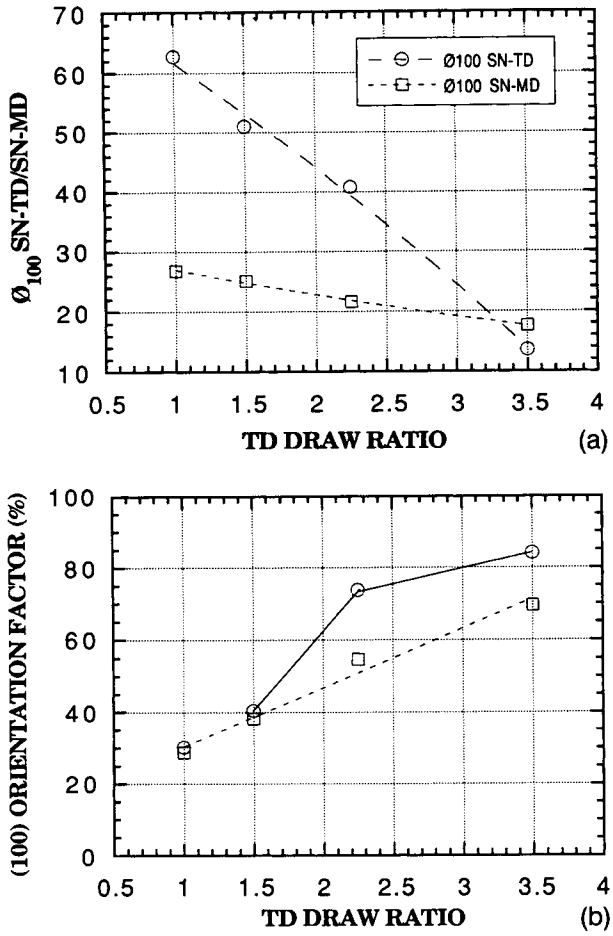

Figure 6 (a) Variation in intensity spread from the (100) crystal plane along the MD and TD (spread in intensity described by the angle ϕ) with TD draw ratios: (○) ϕ along SN–TD; (□) ϕ along SN–MD. (b) Variation in (100) orientation with respect to the film surface in the sequentially stretched annealed and nonannealed films as a function of TD draw ratio: (○) annealed; (□) nonannealed films.

Up to this point, the results of our study and some of the previous work[22] lead to the following conclusions:

The film planarity increases with (1) draw ratio during uniaxial deformation, (2) the total planar biaxial deformation (MDX, TDX), (3) TD deformation of already uniaxially stretched film, and (4) annealing of the films.

In Figure 8, the changes in the orientation of the (100) crystal plane in the film are plotted with the corresponding oxygen permeability. This figure includes data for films stretched sequentially and simultaneously, including both annealed and nonannealed films. The data do not show a relation similar to that seen in Figure 4, suggesting that the

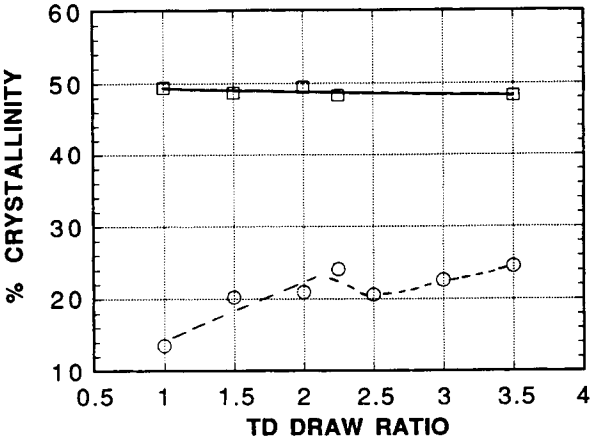

Figure 7 Variation of percent crystallinity for annealed (□) and nonannealed (○) films as a function of TD draw ratio.

orientation of the (100) planes alone is not sufficient to predict the permeability of oxygen.

Before proceeding further, it may be worthwhile to compare the phenyl ring orientation in crystals, and total phenyl ring orientation in both phases, with increasing TD draw. Figure 6(b) shows the (100) crystal plane orientation factor, whereas Figure 9 shows the variation in PROF with TD draw for annealed and nonannealed samples. The (100) crystal plane orientation factor increases in the film plane with TD draw for nonannealed samples. Figure 6(b) shows that there is no increase in (100) plane orientation (over nonannealed samples) upon annealing, until a draw ratio of 1.5× is exceeded.

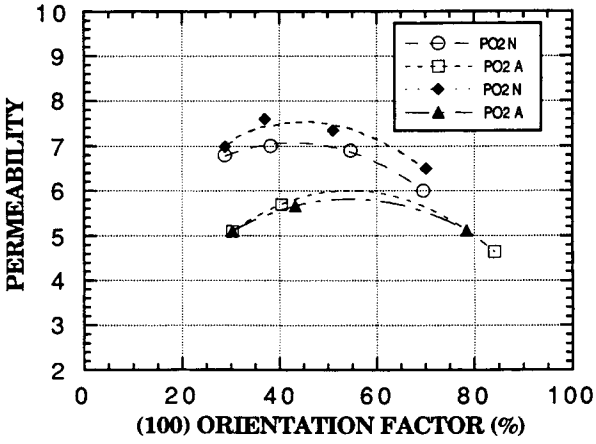

Figure 8 Variation of oxygen permeability for simultaneously and sequentially stretched annealed and nonannealed films as a function of orientation of (100) crystal plane; (○) SEQ nonannealed; (□) SEQ annealed; (♦) SIM nonannealed; (▲) SIM annealed.

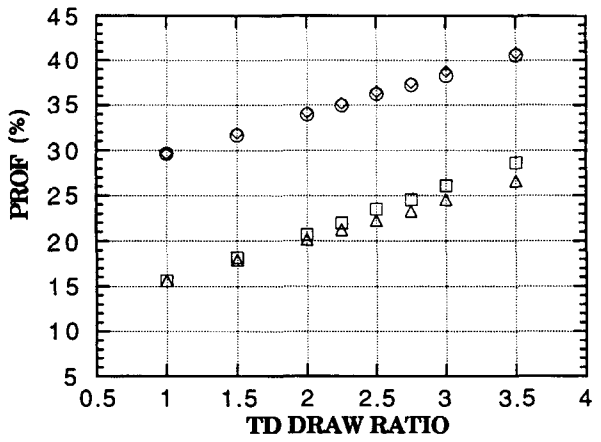

Figure 9 Variation of PROF for simultaneously and sequentially biaxially oriented annealed and nonannealed films: (○) annealed SEQ; (□) nonannealed SEQ; (△) nonannealed SIM; (◇) annealed SIM.

However, as seen from Figure 9, the total phenyl ring orientation is always greater in the annealed samples. The details of this phenomenon will be discussed later.

Amorphous Phase Changes

The major factor governing oxygen permeability is the nature of the amorphous phase. Recently, we have shown that measurements of chain-intrinsic fluorescence can provide information on the nature of the amorphous phase morphology in biaxially oriented PET film.[20] The amorphous orientation ratio along the MD and TD as a function of TD draw ratio is plotted in Figure 10. This figure shows that the orientation ratio along the TD increases with TD draw ratio while it decreases along the MD. A "balance point" is observed at a TD draw of 3.0×. At this orientation, the molecules in the amorphous phase become isotropic in the film plane. After this balance point, the amorphous orientation increases along the TD, with consequent decrease along the MD.

A trend observed in the amorphous orientation ratio as a function of TD draw for annealed samples is also shown in Figure 10 (open points). During annealing, there is apparently a relaxation of the molecules oriented along the TD. The subsequent decrease in TD orientation is accompanied by an increase in MD orientation, suggesting that the restraint on the amorphous molecules by the crystalline network structure that sets up during MD stretching (up to 3.5×) is not destroyed up to a TD draw ratio of 2.0×. Therefore, upon annealing, the amorphous molecules try to assume their original MD (uniaxial) orientation. This is reflected in the (100) plane orientation [Fig. 6(b)]. Above a TD draw ratio of 2.0×, TD AOR remains lower than that observed in non-heat-set samples.

The nature of the amorphous phase is further described by measuring the glass transition temperature using dynamic mechanical analysis; a corresponding parameter is the temperature at which the maximum in tan δ (tan δ MPT) peak occurs. Figure 11 shows the tan δ MPT for annealed and nonannealed samples. In DMA, tan δ–temperature curves, two major peaks are observed for annealed

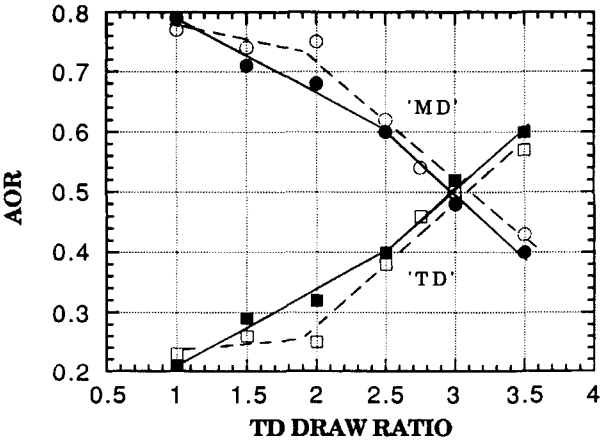

Figure 10 Variation in "amorphous orientation ratio" (AOR) for sequentially stretched annealed and nonannealed films as a function of TD draw ratios: (○) annealed, MD; (●) nonannealed, MD; (□) annealed, TD; (■) nonannealed, TD.

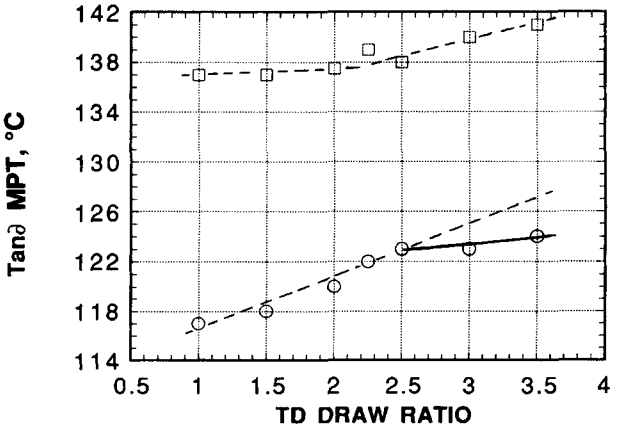

Figure 11 Variation of maximum in the peak temperature of tan δ-temperature curve of DMA in sequentially stretched annealed (□) and nonannealed (○) films as a function of TD draw ratio.

film while only one is noted for nonannealed films. For annealed films, low temperatures tan δ MPT were utilized. The tan δ MPT increases with the TD draw ratio; however, the slopes do not remain constant in both annealed and nonannealed cases. This indicates that the nature of the amorphous phase changes (above a TD draw ratio of 2.5×). For greater insight, the trend of this figure can be compared to the one noted in Figure 10. In nonannealed samples, the TD molecular orientation in the amorphous phase increases with the TD draw ratio. Up to 2.5×, crystallinity slowly increases to 25% (Fig. 7). Thus, the increase in tan δ MPT may be attributed to both increasing crystallinity and to an increase in molecular orientation. The slope of the line in Figure 11 decreases above a TD draw ratio of 2.5×, indicating the development of an effective network structure consisting of loose and taut tie molecules. The decrease in the slope indicates that all molecules in the amorphous phase are not homogeneously deforming. X-ray results confirm a lower population of TD oriented crystals [Fig. 5(b)], which immediately increase with the annealing of the film.[24,25] In this region, there is an increase in the molecular orientation, but at the cost of destruction of some crystallinity,[24] which leads to a decrease in physical cross-links. Thus, the slight increase in tan δ MPT is likely due to an overall increase in the molecular orientation.

In the annealed samples, TD molecular orientation in the amorphous phase does not increase much up to a draw ratio of 2.0× (Fig. 10). In addition, the crystallinity remains almost constant (Fig. 7). Thus, the results are consistent with initial constancy in the value of tan δ MPT (Fig. 11). Above 2.0×, constraint on the oriented molecules increases. Although the percent crystallinity is almost constant, the increase in values of tan δ MPT in Figure 11 is attributed to the development of higher constraint due to relatively higher molecular orientation (Fig. 10). In the present case, the increase in the values of tan δ MPT is not very high.

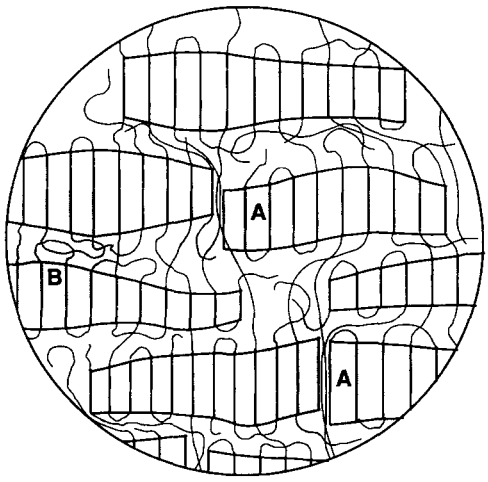

Figure 12 *Schematic representation of film structure* in the local areas developing during annealing below 200°C. Areas marked with "A" show the constraints on molecules imposed by the proximity of crystals, while the area marked "B" indicates the entrapment of loose loops between taut tie molecules.

Thus, on annealing, the incorporation of molecules into crystallites, as well as the proximity of growing crystallites along lateral sides on the oriented molecules, can impose a different type of constraint on the amorphous molecules. The presence of chain ends, loose loops, and molecules totally excluded from crystallization determines the final composition of the amorphous phase. The situation arising after heat treatment below 200°C is depicted in Figure 12. In this case, fibrillar crystals are transformed into lamellar crystals,[23] a phenomenon common in semicrystalline polymers.[26] The areas marked with "A" represent molecules with a greater orientation and experiencing an additional constraint on the amorphous phase due to the proximity of crystallites. The development of such a structural situation will impose different restrictions on segmental motion in different areas. The structural development above 180°C has been shown previously,[25] wherein, due to predominance of melting and recrystallization of crystallites formed by the strain-induced crystallization process, the initial high molecular orientation decreases.

Factors Controlling PROF

PROF increases linearly with the TD draw ratio for sequentially and simultaneously stretched films (Fig. 9). This suggests that, irrespective of the method of stretching, the same heating conditions and stretch ratios lead to an increase in PROF and percent crystallinity to the same extent.

The variation of PROF with birefringence for annealed and nonannealed films is shown in Figure 13. In nonannealed samples, where crystallinity is lower, PROF increases with increasing molecular orientation. After annealing at 200°C, the values of PROF have increased due to an increase in crystallinity. The data at the arrow reflect that, in spite of a similar degree of film crystallinity and birefringence, the value of PROF can be different, due to the different nature of the constraints. The role of molecular orientation can also be deduced from a

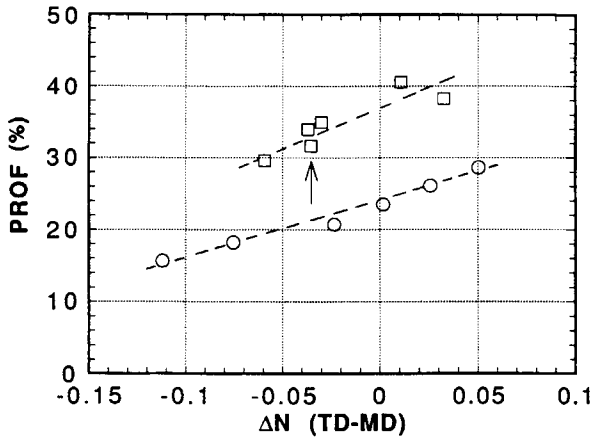

Figure 13 Variation in PROF for sequentially stretched annealed (□) and nonannealed (○) films as a function of birefringence, ΔN.

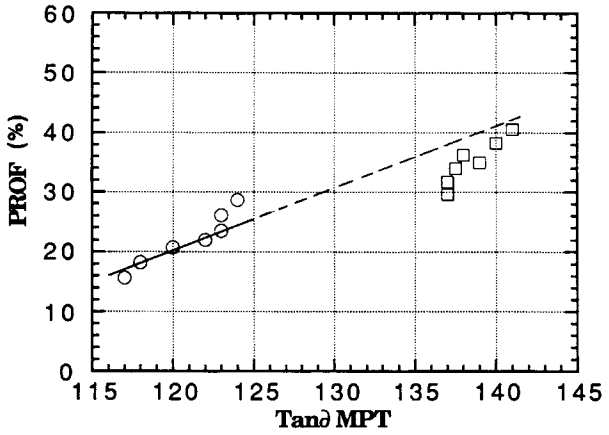

Figure 15 Variation in PROF for sequentially stretched annealed (□) and nonannealed (○) films as a function of maximum peak temperature in tan δ–temperature curves.

comparison of Figures 9 and 10. Thus, it is not surprising that Δn does not show a linear relation with oxygen permeability, as noted by Jabarin.[27]

The variation in PROF with percent crystallinity (Fig. 14) does not show a strictly linear relationship for both annealed and nonannealed samples. Let us first consider the data at the crystallinity close to 50%. In spite of constancy in crystallinity, the films manifest different values of PROF. After annealing, films having a different degree of molecular orientation have the same crystallinity. Even though they have the same crystallinity, the nature of the amorphous phase is different in these films. This is reflected in the values of PROF. The different values of oxygen permeability suggest that the resulting structure has a different constraint on the molecules, i.e., the nature of the amorphous phase is different in various annealed films. It is, therefore, not surprising to find a nonlinear relationship between gas permeability with percent crystallinity in oriented polymeric systems, as seen also in the results of Perkins.[28] The unannealed data at the lower left of Figure 14 also have different molecular orientation and percent crystallinity.

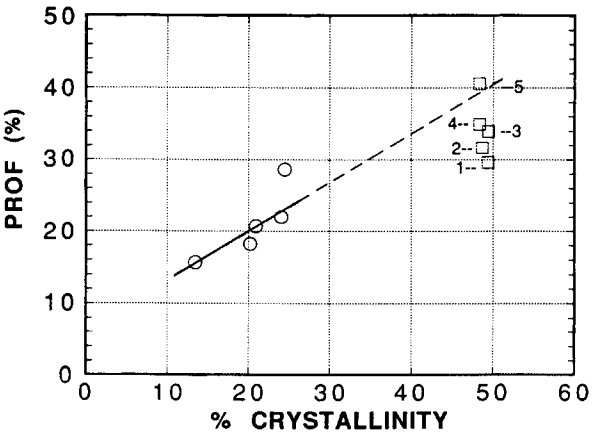

Figure 14 Variation in PROF for sequentially stretched annealed (□) and nonannealed (○) films as a function of percent crystallinity. Numbers indicate draw ratios: (1) 3.5 × 1.0; (2) 3.5 × 1.5; (3) 3.5 × 2.0; (4) 3.5 × 2.25; (5) 3.5 × 3.5.

Tan δ MPT represents contributions of both crystalline and amorphous phases. The observed relation between PROF and tan δ MPT, shown in Figure 15, is linear for the nonannealed samples. Data for samples annealed at 200°C fall below the line extrapolated from the initial values of nonannealed samples. It may be that annealed samples constitute an independent linear relationship. The increase in tan δ MPT, as mentioned previously[29], is due to densification of a network structure (increase in percent crystallinity). At a constant value of tan δ MPT, there could be a different value of PROF due to the different nature of constraint in the amorphous phase (Fig. 12). It is to be noted that the parameters PROF and tan δ MPT are not quite equivalent in monitoring the different natures of the amorphous phase. The results on films annealed at 200°C reflect a change in overall morphology.

The above results lead to the conclusion that most of the changes taking place in the amorphous and crystalline phases, i.e., changes in morphology due to changes in processing conditions, can be inferred from the total phenyl ring orientation factor (PROF). If this is the case, then such a parameter should show a universal type of relationship that could be used to predict film properties.

To check the universality of the relationship, we prepared PET films under a variety of processing and heat-set conditions, including nonstretched, uniaxially, sequentially, and simultaneously biaxially stretched film with different draw ratios and heat treatment with fixed dimensions. The relationship is shown in Figure 16, and the correlation is remarkably good. The value of the intercept (equal to 9) at zero value of PROF is for amorphous films. Extrapolation of the curve to large values of PROF suggests that for achieving zero permeability of oxygen in biaxially oriented films 85–95% of the phenyl rings should lie in the film plane.

DISCUSSION

The uniaxial stretching of PET up to 3.5× forms a network structure consisting of fibrillar or cylindrical crystals.[20,23] A study of network structure deformation perpendicular to the c-axis within the crystals has been carried out. The MD-oriented c-axis of the crystal starts orienting along the TD with increasing TD draw ratio. The crystalline orientation becomes almost isotropic in the film plane at a TD draw ratio of 2.3×. Further stretching along the TD increases the population of TD-oriented crystals, and the effect becomes more pronounced in annealed films. In the course of the c-axis reorientation of crystals during TD stretching, (100) crystal planes preferentially orient in the film plane; hence, the planarity of the film increases during TD stretch. An understanding of the detailed mechanism requires further study; however, a mechanism involving destruction of existing crystals and formation of new crystals is probable. The annealing process also enhances the planarity of the film. The microstructural changes taking place during TD draw of uniaxially (3.5×) drawn film was also confirmed by transmission electron microscopy and by small- and wide-angle X-ray scattering.[23] These studies on annealed samples reveal that MD-oriented lamellar crystals become isotropic in the film plane at the draw ratio of 2.3× and then become predominantly TD oriented at higher TD draw ratios.

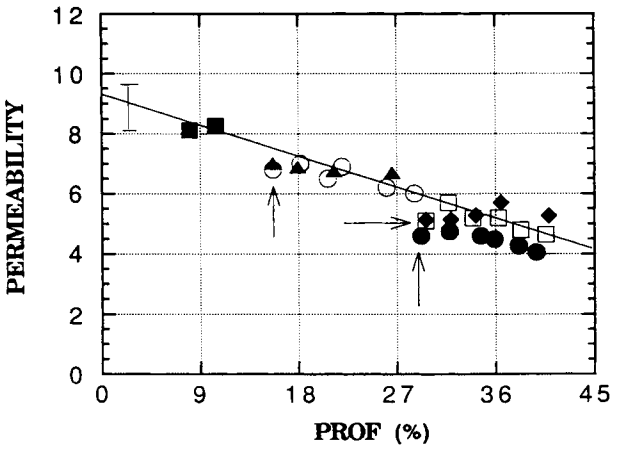

Figure 16 Relation between permeability of oxygen and PROF for the film prepared in a variety of stretching and heat-set conditions: (○) SEQ nonannealed; (□) SEQ annealed at 200°C; (▲) SIM nonannealed; (◆) SIM annealed at 200°C; (●) SEQ annealed at 170°C; (■) nonoriented crystalline film. Arrows indicate values for uniaxially oriented film.

As far as amorphous phase orientation is concerned, TD stretching of uniaxially stretched film (3.5×) converts the MD-oriented amorphous molecules toward the TD. The amorphous orientation lags behind the crystalline orientation and becomes isotropic in the film plane at a TD draw ratio of 3×. At equal draw ratio (3.5 × 3.5), molecules are preferentially oriented toward TD. Thus, on TD stretching, the MD-oriented amorphous material transforms into a TD-oriented amorphous phase. During this transformation, the value of PROF also increases.

Up to a TD draw of 1.5×, the original MD-constrained network structure opens up. On annealing, molecules become reoriented toward the MD (Fig. 10). After heat treatment, crystallization follows the initial crystal orientation. Here, the following four experimental observations are useful in understanding this process: (1) the PROFs of the annealed samples at all TD draw ratios are higher than the values of nonannealed samples (Fig. 9); (2) the orientation of the molecular axis (c-axis) within crystals for annealed and nonannealed film remain unchanged up to a TD draw ratio of 1.5×; (3) intrinsic fluorescence shows that up to a TD draw ratio of 2.0× molecules in the amorphous phase reorient along the MD on annealing at 200°C; and (4) the crystallinity of all annealed samples attains the same value independent of TD draw ratio (Fig. 7).

The changes taking place in the amorphous phase during the TD draw were also followed by DMA. The decrease in the slope of the tan δ MPT–TD draw curve (Fig. 11) above a TD draw ratio of 2.5× suggests the growth of taut tie molecules among the crystallites. The development of this type of morphology restricts further homogeneous stretching of the relatively relaxed amorphous phase. A similar inference was proposed in a previous study.[22] The values of tan δ MPT are controlled by percent crystallinity, molecular orientation, and the nature of

constraint imposed by the crystallites. Thus, incorporation of molecules into both existing and new crystals, as well as the proximity of growing crystallites along lateral sides of the oriented molecules, can impose a different type of constraint on the oriented amorphous molecules. The development of such structural situations will impose numerous restrictions on segmental motion in different local areas, which, in turn, will affect the rate of gas diffusion through the film.

The oxygen permeability initially increases up to a TD draw of 1.5× (Fig. 3), suggesting the opening of the initial network structure in uniaxially drawn films. It then starts decreasing with TD draw. The decrease is not significantly high and is lower in the films annealed at 170°C than at 200°C. This indicates a marked change in the morphology upon annealing at 200°C. Such a change can be attributed to competition among several processes; a structural model explaining such behavior has been discussed previously by the author.[25]

PROF does not show a linear relation with molecular orientation, crystallinity, tan δ MPT, or birefringence. This behavior is similar to that seen for the permeability of gases with the above parameters. Even though tan δ MPT is dependent on percent crystallinity and molecular orientation, it is not strictly equivalent to PROF (Fig. 15). These properties can approach equivalency depending on the nature of constraint in the amorphous phase (Fig. 12).

Thus, PROF represents the phenyl ring orientation in the crystalline and amorphous phases in most morphological situations. Information regarding phenyl ring orientation should echo the degree of molecular orientation achieved in the films and various types of constraint imposed by the growth of crystallites. As PROF reflects changes taking place in the morphology on changing processing conditions, it can be useful for establishing processing–property–morphology relationships.

The relation between oxygen permeability and (100) plane orientation for the annealed and nonannealed films stretched by sequential and simultaneous stretching processes is not linear. Thus, for describing oxygen permeability, the contribution of phenyl ring orientation from both crystalline and amorphous phases is required. The contribution from the crystalline state represents the change in crystallinity due to heat treatment, while the contribution from the amorphous phase represents changes taking place in the amorphous phase morphology.

Experimental values of oxygen permeability obtained from films stretched by sequential and simultaneous biaxial stretching processes and heat-set at different temperatures, as well as nonstretched crystalline film, show good correlation with PROF (Fig. 16). Most of the data falls on a line that has an intercept of 9.00 cc-mil/100 in.^{2} 24 h-1 atm. at zero value of PROF. The value of the intercept, which reflects the value of completely isotropic amorphous films, is also influenced by the diethylene glycol content (DEG), nature of additives, and molecular heterogeneity. In the present study, the values of PROF were calculated using refractive indices along the MD, TD, and thickness direction. For greater accuracy, values could be measured along maximum and minimum orientation directions. Also, there are other approaches to calculate values of PROF for biaxially oriented films,[9,18] but refractive index measurements are easy, simple, and less expensive. A unique relation of this type can be established for other gases, water vapor, and other film properties.

A question arises: Which morphology causes a deviation from linearity in relation to oxygen permeability and PROF. The following observations can give some insight into this question:

In spite of similar values of PROF after annealing at 170 and 200°C, the corresponding values of oxygen permeability are different (Figs. 3 and 16). Furthermore, our study on the balanced PET films annealed at different temperatures[25] shows that at 180°C the oxygen permeability attains a minimum value while tan δ MPT manifests a maximum value. The permeability minimum at 180°C was also noted by Perkins.[28] This clearly indicates a different morphology above and below 180°C, which signifies the development of a different type of constraint on the amorphous phase. It should be noted that the specific nature of the amorphous phase is determined from the competition among various processes like rate of crystallization, molecular relaxation, solid-state thickening processes, and melting and recrystallization processes at a given annealing temperature. In the temperature range where the crystallization rate is higher, molecular relaxation processes will be minimized and crystallization processes will involve oriented molecules. Here the amorphous molecules try to maintain their initial orientation. In such conditions, the interconnecting tie molecules among the crystals will be more constrained than at crystallization above 200°C. The morphological situation below 180°C is depicted in Figure 12. Looking at the experimental evidence, it is seen that

the values of PROF measured for the films annealed at 170 and 200°C is not different but the permeability of oxygen is lower at 170°C, suggesting that the type of constraint experienced by the molecules may be different. The exact mechanism is difficult to confirm, but one possibility of imposing additional constraint on the amorphous phase by the proximity of the crystals is shown by the areas marked "A" in Figure 12. In such a situation, increased constraint can occur without a net increase in PROF.

Let us examine the results in Figure 16 on oxygen permeability in uniaxially oriented films (arrows). These values are lower than most of the biaxially oriented films. The results of Matsumoto et al.[18] also suggest higher molecular constraints in uniaxially oriented PET film in comparison to their biaxially oriented PET films.

The proximity of crystallites can play an effective role in developing additional constraint when crystallization is carried out from the highly oriented state. Their role diminishes as processes such as melting and recrystallization predominate above 200°C. The schematic presentation of such a situation was shown in a previous publication.[25] This type of morphology can also become predominant in highly uniaxially oriented film, a view supported from the results shown in Figure 3 where the value of oxygen permeability is lower in uniaxially oriented film (TD draw ratio = 1) than in biaxially oriented film with a planar draw ratio of 3.5 × 1.5.

CONCLUSIONS

The total phenyl ring orientation factor PROF represents phenyl ring orientation in the crystalline and amorphous phases, which gives a measure of the molecular orientation and the nature of constraint imposed by the crystallites. The constraints on the molecules control segmental mobility and, thereby, the oxygen permeability. Since PROF reflects changes taking place in the morphology with changing processing conditions, it can be useful for establishing processing–property–structure relationships.

At a particular stretch rate and temperature, the total phenyl ring orientation depends upon the planar draw ratio (MD × TD) and heat-set conditions and is independent of the stretching process (i.e., sequential or simultaneous).

Oxygen permeability of biaxially oriented PET films can be effectively correlated with PROF. It gives a useful relationship for biaxially oriented films, which, in most cases, can be used to predict the film properties. The orientation of (100) crystal planes containing the phenyl ring does not show a unified relation with oxygen permeability.

The oxygen permeability of biaxially oriented film is determined mainly from the orientation achieved in the first drawing and by the heat-setting temperature. TD stretching marginally improves the permeation resistance due to the MD-oriented amorphous phase being transformed toward the TD during the TD drawing process. Heat-setting induces the physical tie points (crystallinity, which constrains the amorphous molecules). A very effective constraint develops in the temperature range of maximum crystallization rate. However, in this case, the PROF value does not increase appreciably. For PET, the optimum temperature for heat-setting with fixed dimensions is in the range of 180–190°C.

Below a particular TD draw ratio, the annealing of biaxially oriented films causes reversion to initial uniaxial molecular orientation, suggesting that the initially formed (uniaxial) crystalline network structure opens up but is not totally destroyed. However, in this process, the original constraint of uniaxial orientation as well as the corresponding decrease in oxygen permeability cannot be attained after only slight TD stretching. For attaining the optimum permeation resistance by TD drawing, it is necessary to achieve an effective network structure along the TD.

The author is thankful to Dr. M. Keating, Dr. F. Wilson, M. Simpson, and J. Cooper for their help in pursuing some of the experiments and to Drs. Ross Lee, J. M. Schultz, and Bill Hurley for the inspiration to undertake this study program.

REFERENCES

1. V. Stannett, in *Diffusion in Polymers,* J. Clark and G. S. Park, Eds., Academic Press, London, 1968.
2. W. J. Koros, Ed., *Barrier Polymers and Structure,* ACS Symposium Series 423, American Chemical Society, Washington, DC, 1990.
3. W. R. Vieth, *Diffusion in and through Polymers,* Hanser, Munich, 1992.
4. M. Salame and S. Steingiser, *Polym. Plast. Eng.,* **8**(2), 155 (1977).
5. A. Peterlin, *J. Macromol. Sci.-Phys. B,* **11**(1), 57 (1975).
6. W. E. Brown and P. T. DeLassus, *Polym. Plast. Tech. Eng.,* **14**(2), 171 (1980).
7. N. Swaroop and G. Gordon, *Polym. Eng. and Sci.,* **20,** 78 (1980).
8. J. A. Slee, G. A. J. Orchard, D. I. Bower, and I. M.

Ward, J. Polym. Sci Part B Polym. Phys. **27,** 71 (1989).
9. G. A. Orchard, P. Spiby, and I. M. Ward, *J. Polym. Sci. Polym. Phys. Ed.,* **28,** 603 (1990).
10. R. M. Gohil and J. Petermann, *J. Polym. Sci. Polym. Phys. Ed.,* **17,** 525 (1979).
11. J. E. Sax, V. P. Thalacker, T. E. Boettcher, and E. G. Larson, *Radiat. Phys. Chem.,* **31**(4), 887 (1988).
12. Mocon Oxtran, Operating Manual, Modern Control Inc., Minneapolis, Minnesota.
13. L. E. Alexander, *X-ray Diffraction Methods in Polymer Science,* Robert E. Krieger Publishing Co., Malabar, FL (1979).
14. M. Cakmak, J. L. White, and J. E. Spruiell, *J. Polym. Eng.,* **6,** 291 (1986).
15. S. R. Hu and M. Xu, *Gaofenzi Tongxum,* **2,** 157 (1985).
16. N. Yoshihara, A. Fukishima, Y. Watanabe, A. Nakai, S. Nomura, and H. Kawai, *Sen-i-Gakkaishi,* **37,** 387 (1981).
17. C. J. Heffelfinger and P. G. Schmidt, *J. Appl. Polym. Sci.,* **9,** 2661 (1965).
18. K. Matsumoto, H. Ieki, and R. Imamura, *J. Fiber Sci. (Jpn),* **27**(2), 516 (1971).
19. M. Hennecke, A. Kud, and J. Fuhrmann, *J. Colloid Polym. Sci.,* **265,** 674 (1987).
20. R. M. Gohil and D. Salem, to appear.
21. B. Clauss and D. R. Salem, *Polymer,* to appear.
22. C. Heffelfinger and R. L. Burton, *J. Polym. Sci.,* **47,** 289 (1960).
23. H. Chang, J. M. Schultz, and R. M. Gohil, to appear.
24. K. Matsumoto, U. Izumi, and R. Imamura, *J. Fiber Sci. (Jpn),* **28**(6), 179 (1972).
25. R. M. Gohil, in *Proceedings of the 49th Annual Meeting of Electron Microscopy Society of America,* San Francisco, CA, 1991, p. 1056.
26. J. M. Schultz, J. S. Lin, R. W. Hendricks, J. Petermann, and R. M. Gohil, *J. Polym. Sci. Polym. Phys. Ed.,* **19,** 609 (1981).
27. S. A. Jabarin, *Polym. Eng. & Sci.,* **24**(5), 376 (1984); **31**(14), 1071 (1991).
28. W. Perkins, *Polym. Bull.,* **19,** 397 (1988).
29. K. Matsumoto, Y. Hosoda, Y. Izumi, and R. Imamura, *J. Fiber Sci.,* **30**(9), 424 (1974).

Received June 16, 1992
Accepted August 6, 1992